VIRTUAL AND PHYSICAL PROTOTYPING
2023, VOL. 18, NO. 1, e2259871 (9 pages)
https://doi.org/10.1080/17452759.2023.2259871

Heterogeneous microstructure and mechanical properties of Monel alloy parts repaired by laser directed energy deposition

Ze Chen[a], Shubo Gao[a], Zhuohong Zeng[a], Yung Zhen Lek[a], Ming Gao[a], Zhongmin Xiao[a], Sastry Yagnanna Kandukuri[b] and Kun Zhou [a]

[a]Singapore Centre for 3D Printing, School of Mechanical and Aerospace Engineering, Nanyang Technological University, Singapore, Singapore; [b]DNV AS, Oslo, Norway

ABSTRACT

Additive manufacturing (AM) offers the advantages of direct near-net-shape production, reduced material waste, and shortened production lead time, showing great potential to revolutionise the manufacturing industry. The flexible movements of the deposition head and the build platform allow directed energy deposition (DED) to conduct the repair process of damaged high-value metallic parts. However, the resulting heterogeneous microstructure and its effect on the mechanical properties of the repaired parts have not been widely realised. In this work, the repair of Monel alloy parts, known for their excellent mechanical properties and high corrosion resistance, was conducted by the laser-DED process with low and high laser power settings, respectively. Different from the fine, equiaxed grains in the original part, the as-deposited Monel alloy consists of large columnar grains. The mechanical performance across the interface between the original and newly deposited material was tested and analysed along horizontal and vertical loading directions. The yield strength and elongation of repaired Monel alloy parts were 409.1 MPa and 35.2% along the horizontal loading direction, which both significantly surpass the corresponding values along the vertical loading direction. This study lays the groundwork for designing a laser-DED process to achieve high performance for repaired metallic parts.

ARTICLE HISTORY
Received 13 June 2023
Accepted 12 September 2023

KEYWORDS
Directed energy deposition; Repair; Monel alloy; Heterogeneous microstructure; Mechanical property

1. Introduction

Additive manufacturing (AM) has become a revolutionary technology promoting advancement in various manufacturing industries, including aerospace, automotive, and biomedical sectors [1–4]. The layer-by-layer fabrication mode imparts AM with significant advantages, such as complex geometries [5], reduced waste and cost [6], and shortened lead times [7,8]. As one of the primary metal AM techniques, directed energy deposition (DED) utilises a focused beam of energy source (laser or electron beam) to simultaneously melt and deposit the material onto a substrate [9–11]. The unique features of the DED process include high deposition rates, large printing scale, and flexible relative motion between the deposition head and substrate [12]. These features enable the use of DED for the rapid repair of large and expensive components in industries, allowing them to be quickly returned to service.

The replacement of damaged or worn-out parts can be costly and time-consuming, leading to material wastage and decreased production efficiency. However, utilising the DED technology to repair damaged components presents an opportunity to significantly minimise maintenance costs and reduce material waste. Additionally, the lower heat input as compared to welding processes results in lower residual stresses and distortion, and its automation capabilities enable precise and efficient repairs that outperform conventional repair methods [13]. Hence, the repair conducted by DED could significantly minimise the maintenance cost, material wastage, and machine downtime [14], especially for those parts with intricate geometries.

Monel is a group of nickel–copper alloys that are known for their high resistance to corrosion, excellent thermal conductivity, and good mechanical properties [15–17]. Thus, Monel alloys are widely used in corrosive and other harsh environments for marine and offshore

CONTACT Shubo Gao shubo.gao@ntu.edu.sg Singapore Centre for 3D Printing, School of Mechanical and Aerospace Engineering, Nanyang Technological University, 50 Nanyang Avenue, Singapore 639798, Singapore; Kun Zhou kzhou@ntu.edu.sg Singapore Centre for 3D Printing, School of Mechanical and Aerospace Engineering, Nanyang Technological University, 50 Nanyang Avenue, Singapore 639798, Singapore

applications [18,19]. The research on Ni–Cu alloys fabricated by AM has attracted significant interest in recent years. For example, Raffeis et al. [20] employed laser powder bed fusion (LPBF) to produce a variant of Monel alloys that showed anisotropic mechanical properties. Marenych et al. [21] utilised the wire-DED process to fabricate a Monel K-500 alloy age-hardened by nano-precipitates. Chen et al. [22] investigated the grain morphology evolution in DED-produced Monel alloys as a function of process parameters. Despite the growing trend of fabricating Monel alloys by AM, the work employing laser-DED to repair Monel parts still remains limited. The differences in microstructural features between the wrought and AM-deposited parts may result in different mechanical properties and deformation mechanisms. Hence, understanding the microstructural evolution and mechanical performance of repaired commercial components employed in the maritime industry is of significant interest.

This work investigated the application of laser-DED on the repair of Monel parts with wrought microstructure. A damaged Monel K-500 component was first machined to obtain a smooth surface. Monel K-500 alloy powder particles were fused and deposited on this surface by DED using two laser power settings. The microstructure and mechanical performance were analysed across the interface between the original and newly deposited material. The effect of heterogeneous microstructure on the tensile properties of the repaired parts was investigated along two different loading directions. This work provides insights into the microstructure design of repaired parts to achieve high performance by varying DED parameters and understanding of the heterogeneous mechanical behaviour of the bonding interface.

2. Materials and methods

2.1 Sample preparation

The Monel K-500 alloy part was repaired through a five-axis coaxial powder-fed laser-DED machine (BeAM Magic 800). The laser beam was focused at a spot size of 1.2 mm. The powder employed in this work was Industrial-grade spherical Monel K-500 powder (Sandvik Osprey Ltd, UK) with a particle size ranging from 53 μm to 150 μm and chemical composition as shown in Table 1. The DED-repair process was performed using the same scanning speed of 1800 mm/min, hatch spacing of 1.5 mm, and raster scanning strategy [23] to ensure the deposited part with a low density of defects. Two different laser power values, 1200 and 1500 W, were selected to investigate the influence of process parameters on the microstructure and properties of the parts repaired by DED. A machined Monel K-500 baseplate with wrought microstructure was taken as the original part for the repair, as illustrated in Figure 1a. To reduce the internal stress, the Monel K-500 plate (hardened condition) underwent a quick annealing (1110 °C for 15 min) prior to the DED process.

Table 1. Chemical composition of the as-received Monel K-500 powders (in wt.%).

Cu	Al	Fe	Mn	Ti	O	Ni
30.0	2.35	1.2	1.1	0.82	0.01	Bal.

2.2 Microstructure characterisation

The repaired Monel K-500 samples for microstructure characterisation and mechanical tests were selectively cut from the baseplate by electrical discharging machining. The microstructure was characterised by optical microscopy (OM; LEXT OLS4100, Olympus, Japan), scanning electron microscopy (SEM; JEOL JSM-7600F), and electron backscatter diffraction (EBSD) techniques. EBSD was employed to assess crystallographic orientation, grain boundary statistics, and local misorientation of the repaired microstructure, using a step-size of 1 μm. All EBSD maps were processed using the software Channel 5 (Oxford Instruments). The average grain (both equiaxed and columnar) size was calculated as circle equivalent diameter of grains and area-weighted by the analysis software.

2.3 Tensile tests

The tensile plates with a gauge area of 10 mm in length, 4 mm in width, and 3 mm in thickness (more details seen in Figure 3c) were cut from the original, as-deposited, and repaired interface parts respectively, along the directions that are parallel and perpendicular to the interface, as shown in Figure 1b. To evaluate the mechanical performance of the repair bonding, the fusion interface between the as-deposited part and the original part was maintained at the centre of the tensile coupons. The tensile coupons were tested at a strain rate of 0.001 s^{-1} at room temperature by a uniaxial tester (Shimadzu AGX 10 KN, Japan) with a TRViewX video extensometer. Each microstructure and loading direction were repeated at least three times. To explain the different tensile behaviour along the respective loading directions, in-situ tensile testing was conducted at the same strain rate on a 5 kN Deben micro-test stage under the observation of OM. The in-situ tensile coupons were polished like a mirror surface.

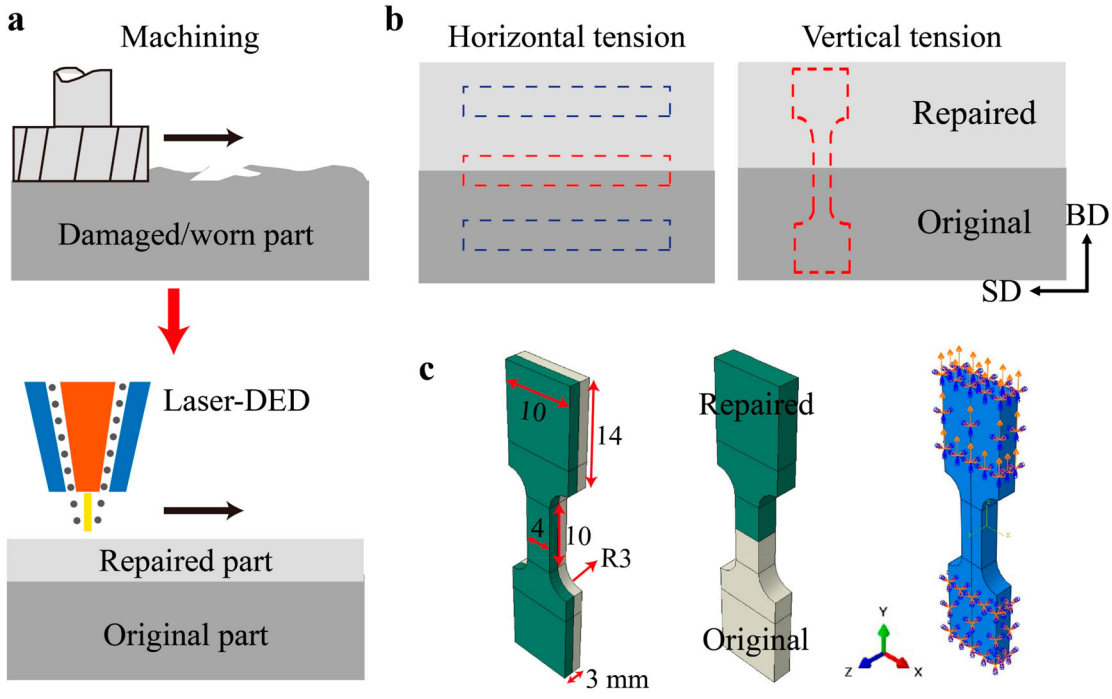

Figure 1. Repair of Monel alloy parts and sample preparation. (a) Schematic of the repair process by laser-DED. (b) Illustration of tension coupon extraction. (c) Dimensions of tensile coupon and finite element analysis model for the tension behaviour.

2.4 Numerical simulation

The numerical simulation was conducted using finite element analysis (FEA) in software (ABAQUS Explicit 2022). The model was created in Abaqus CAE in accordance with the dimension of the tensile coupons used in the experiments. The tensile coupon containing repaired interface was modelled as a composite structure, in which two material properties were assigned to the original half and the as-deposited half (Figure 1c). The material parameters (Table 2) for the single component in the FEA simulation were derived from the experimental tensile results. The ductile damage phenomenon was modelled using Abaqus's metal ductile damage evolution model [24]. The FEA model was meshed with C3D8R elements with an element size of 0.1 mm in the gauge length region. The loading and boundary conditions were established according to the tensile testing in which the bottom grip section was in encastre boundary condition while the top grip section was constrained to move in the *y*-direction only (Figure 1c).

Table 2. Material properties of the composite tensile coupon.

	Original part	As-deposited part (Horizontal)	As-deposited part (Vertical)
Density (t/m^3)	8.5	8.44	8.44
Young's modulus *E* (GPa)	163.5	96.9	214.8
Yield strength (MPa)	503.5	358.4	305.0
Poisson's ratio *v*	0.3	0.3	0.3

3. Results and discussions

Figure 2 shows the OM images and EBSD inverse pole figure (IPF) maps of the repaired Monel alloys processed by laser of 1200 and 1500 W respectively. The OM images shown in Figure 2a,d suggest that the higher laser power generated a larger melt pool. Both the low and high laser power achieved good deposition quality, which is reflected in Figure 2b,e. Only a few small-size pores were visible in the deposited part. Importantly, no cracks, one type of commonly observed defect in joining materials [25], appeared around the interface during the DED-repair process.

As shown in the EBSD IPF maps (Figure 2c,f), the original microstructure of the Monel alloys consisted of fine equiaxed grains with an average grain size of 43 µm. In the as-deposited parts, the much larger columnar grains occupied the microstructures. Owing to the higher power employed (1500 W), the larger melt pools formed during the DED process resulted in a relatively lower cooling rate, which explains a larger columnar grain size (hundreds of µm) in Figure 2f compared to

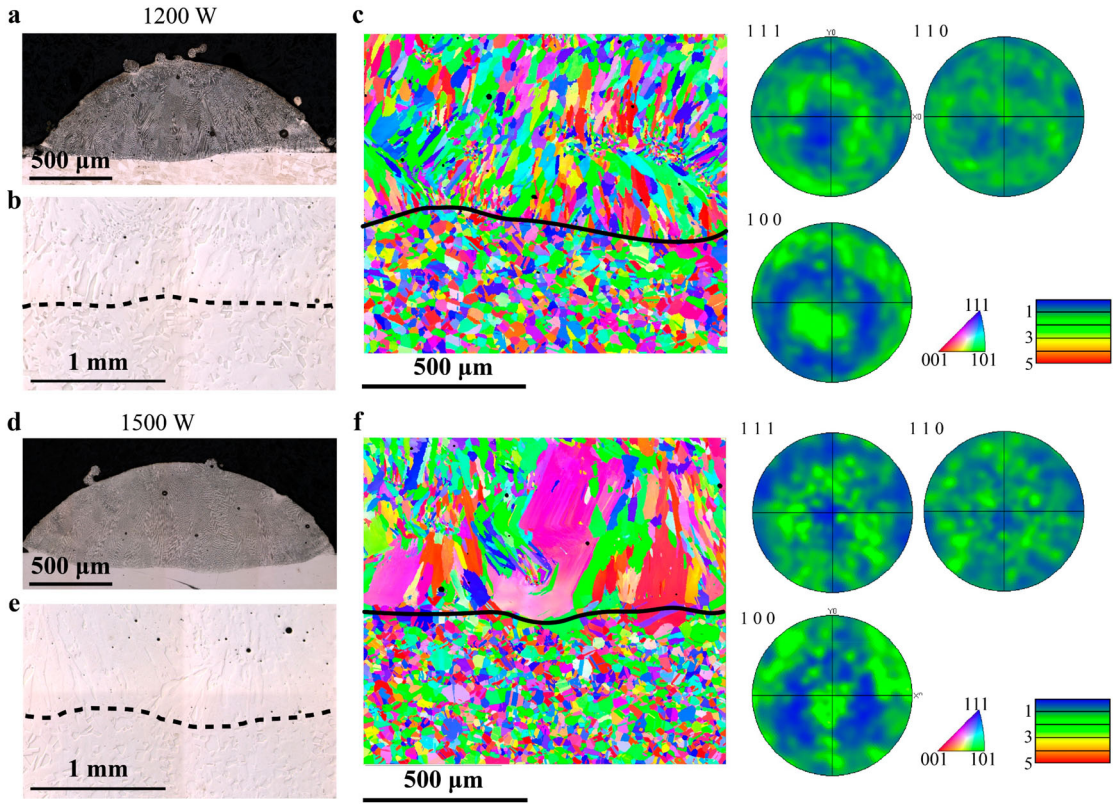

Figure 2. Repaired microstructure characterised by OM and EBSD. (a) and (d) show the single bead deposition of Monel K-500 on the original part. (b) and (e) illustrate the deposition quality by 1200 and 1500 W laser power. (c) and (f) demonstrate the heterogeneous microstructure and the weak crystallographic texture of the repaired Monel K-500.

that in Figure 2c. Another noteworthy point is that the fraction of equiaxed grains was higher in the microstructure of low power (1200 W) deposition (as indicated by the white circles in Figure 2c). This is attributed to the decreased ratio of thermal gradient and solidification rate by lower power energy input, promoting the transformation from columnar to equiaxed grains [22]. The as-deposited microstructures resulted from both laser power settings exhibited no strong crystallographic texture, which is proved by the pole figures shown in Figure 2c,f.

Tensile tests of the original wrought material and two as-deposited DED build samples were conducted along horizontal and vertical directions, respectively, as shown in Figure 3a,b. Based on the Hall–Petch relationship [26], the strength of metallic materials is significantly sensitive to grain size. Because of the equiaxed morphology and much smaller size of grains in the original hardened wrought Monel K-500, its yield strength (YS) and ultimate tensile strength (UTS) reached 583.1 and 949.7 MPa, respectively, and can be considered equivalent along two different loading directions. By comparison, the as-deposited Monel K-500 alloys exhibited higher ductility but much lower YS and UTS, as shown in Figure 3a,b. The as-deposited microstructures exhibited anisotropic tensile behaviour owing to the dominated columnar grain morphology. Along the horizontal loading direction, the as-deposited Monel K-500 alloys showed higher strength than those being tested along the vertical loading direction. This originates from the higher density of grain boundaries blocking the movement of dislocations along the horizontal direction. Since the average grain size was smaller in low power deposition, the strength of 1200 W produced Monel K-500 alloy was relatively higher than that of 1500 W produced alloy along both loading directions.

To evaluate the bonding strength of the repaired interface, tensile tests were also performed on the Monel K-500 samples containing the bonding interfaces. As shown in Figure 3 and Table 3, the YS and UTS of the repaired Monel K-500 fell in between the values of fully original wrought and as-deposited microstructures. Since the strength of 1200 W deposited microstructure was higher than that of 1500 W deposited microstructure, the strength of 1200 W repaired Monel alloys was correspondingly higher along both loading directions. When the loading direction was vertical, apart from the lower strength compared to that of the horizontal direction, one noteworthy point is the ductility was significantly reduced (Figure 3b). Nevertheless, the tensile

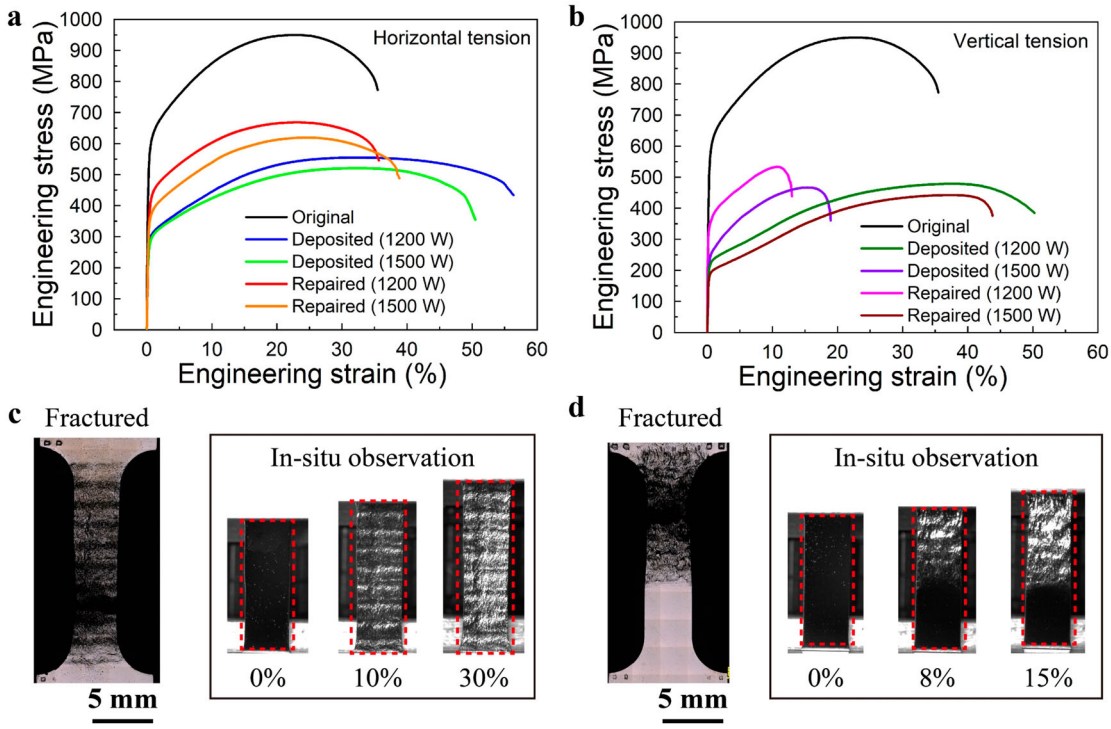

Figure 3. Tensile behaviours of repaired heterogeneous samples. (a) Stress-strain curves for Monel K-500 alloys tensioned along the horizontal direction. (b) Stress-strain curves for Monel K-500 alloys tensioned along the vertical direction. Fractured Monel K-500 samples tensioned along (c) horizontal and (d) vertical directions with corresponding in-situ observations showing strain localisation captured by OM.

fracture of vertical loading occurred in the newly deposited part, which proves the good bonding quality of the repair interface.

To explain the reduced ductility along the vertical loading direction, the in-situ tensile tests were carried out under the observation of OM. The plastic deformation increased the roughness of the polished surface of the tensile coupons. Thus, the surface brightness can reflect the strain distribution. As shown in Figure 3c,d, the in-situ tensile behaviour indicates that the strain distributions are completely different in the two respective loading directions. The strain distribution was uniform over the whole gauge area upon the tensile deformation along the horizontal direction. On the contrary, the plastic strain initiated and accumulated in the deposited part when the loading direction was vertical. Moreover, the original part did not show an obvious plastic strain signal under such conditions. This significant strain heterogeneity originates from the huge difference in the tensile properties between the two single microstructure-components.

Table 3. Tensile properties of Monel K-500 parts repaired by laser-DED.

SN	Condition	Sample	UTS (MPa)	YS (MPa)	Elongation (%)
1	Repaired	1200 W-H	654.8 ± 19.6	409.1 ± 31.3	35.2 ± 3.8
2		1200 W-V	544.7 ± 11.6	353.7 ± 17.2	11.7 ± 2.9
3		1500 W-H	610.3 ± 8.3	334.8 ± 11.9	36.8 ± 3.6
4		1500 W-V	473.9 ± 6.6	261.5 ± 16.1	14.5 ± 4.6

The FEA were performed to understand the tensile behaviours along the horizontal and vertical directions, up to the engineering strain of 30% and 15%, respectively. The von Mises stress distribution shown in Figure 4a demonstrates higher stress locating in the original wrought part when the loading direction is horizontal, to accommodate the strain compatibility between the hard original wrought part and soft deposited part. Due to the strain hardening, the stresses in both parts correspondingly increase as the plastic deformation continues. If the loading direction is vertical, owing to the much lower YS, the deposited part yields first and continues to be plastically deformed alone. However, as the stress in the deposited part reaches its UTS (544.7 MPa), the value is still lower than the YS (583.1 MPa) of the original wrought material, as shown in Figure 4. Therefore, the plastic strain exclusively concentrates in the deposited part upon the vertical tensile loading. The fracture position of the tensile sample is consistent with the strain accumulation simulated by FEA (Figure 3d and Figure 4d).

To further elucidate the heterogeneous mechanical behaviour of the repaired Monel K-500 alloy, EBSD was

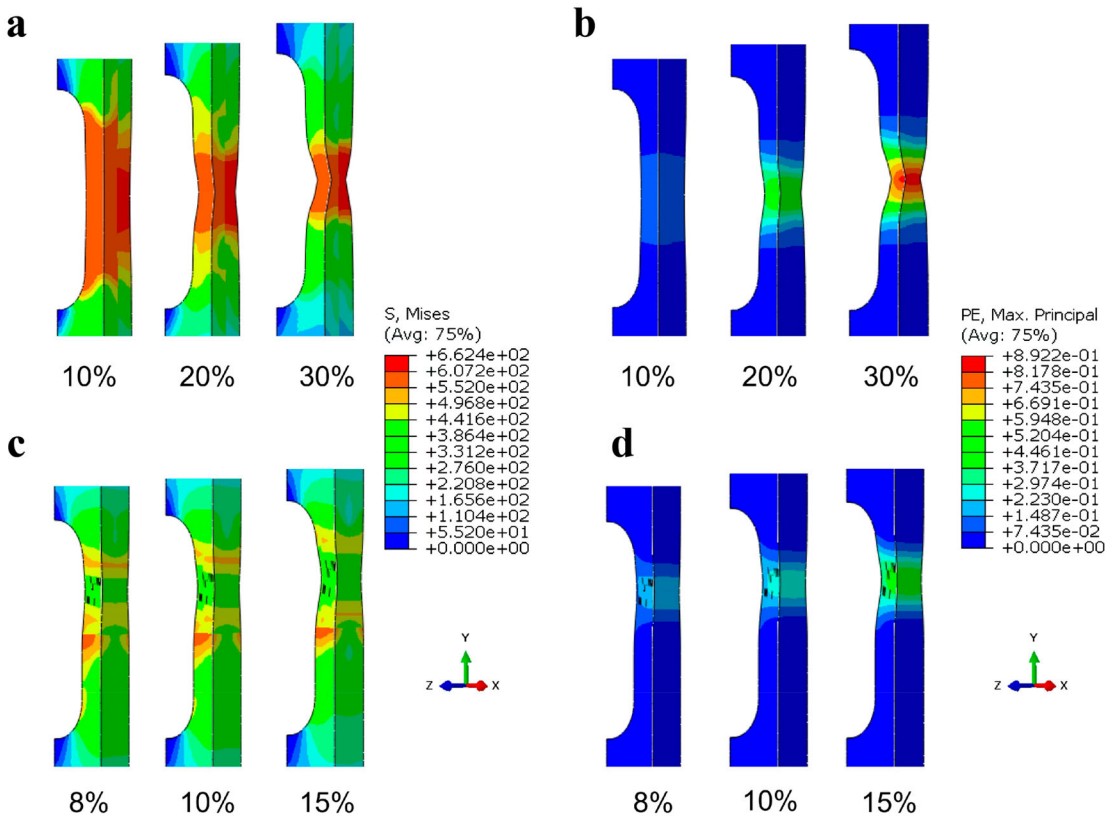

Figure 4. Finite element analysis of the samples repaired by 1200 W laser. Von Mises stress distribution for (a) horizontal and (c) vertical sample models. Plastic strain distribution for (b) horizontal and (d) vertical sample models.

carried out to analyse the deformed microstructures of two samples which were loaded along different directions, as shown in Figure 5. Before the deformation, the original part was dominated by a high-density of high angle grain boundaries (HAGBs, > 15°) and twin boundaries. Different from the original wrought microstructure, the deposited microstructure only showed high-density HAGBs and a few low angle grain boundaries (LAGBs, 2–15°). Kernel Average Misorientation (KAM) maps obtained by EBSD qualitatively reflect the distributions of dislocations stored in the microstructure [27]. The KAM map shown in Figure 5a indicates that the dislocation density in the repaired Monel K-500 alloy mainly concentrated along the fusion line before the deformation, because of the high thermal stresses generated during the DED process [28]. The microstructure shown in Figure 5b was extracted from the fractured tensile sample along the horizontal direction. Additional LAGBs appeared in both original and deposited parts upon the tensile deformation. The KAM map in Figure 5b also proves the uniform distribution of the generated dislocations across the bonding interface. In contrast, in Figure 5c, the significantly increased fraction of LAGBs and density of dislocations in the deposited part demonstrates the severe strain accumulation when the loading direction is perpendicular to the interface. The EBSD maps extracted from the original part of the fractured sample (Figure 5c) exhibit no change compared to those shown in Figure 5a, indicating no plastic deformation in the original part. All these characterisation results well match the experimental and simulation results of the tensile behaviours shown in Figure 3 and Figure 4.

To further elaborate the deformation behaviour of the respective tensile samples, the corresponding fracture surfaces are shown in Figure 6. In Figure 6a, the fracture surface along horizontal direction shows a combination of dissimilar morphologies. The as-deposited part is composed of dimples while the original part contains cleavage planes. This phenomenon is consistent with the results shown in Figure 3 that the as-deposited Monel alloy exhibits a higher ductility. By comparison, owing to the plastic strain accumulating in the as-deposited part when the loading direction is vertical, the fracture surface shown in Figure 6b exhibits a uniform, dimpled pattern corresponding to the homogeneous microstructure in the fracture position.

Although the repair by laser-DED achieved a good interfacial bonding in this work, the mechanical properties of the repaired components were still lower than the performance of original part. The deformation process is

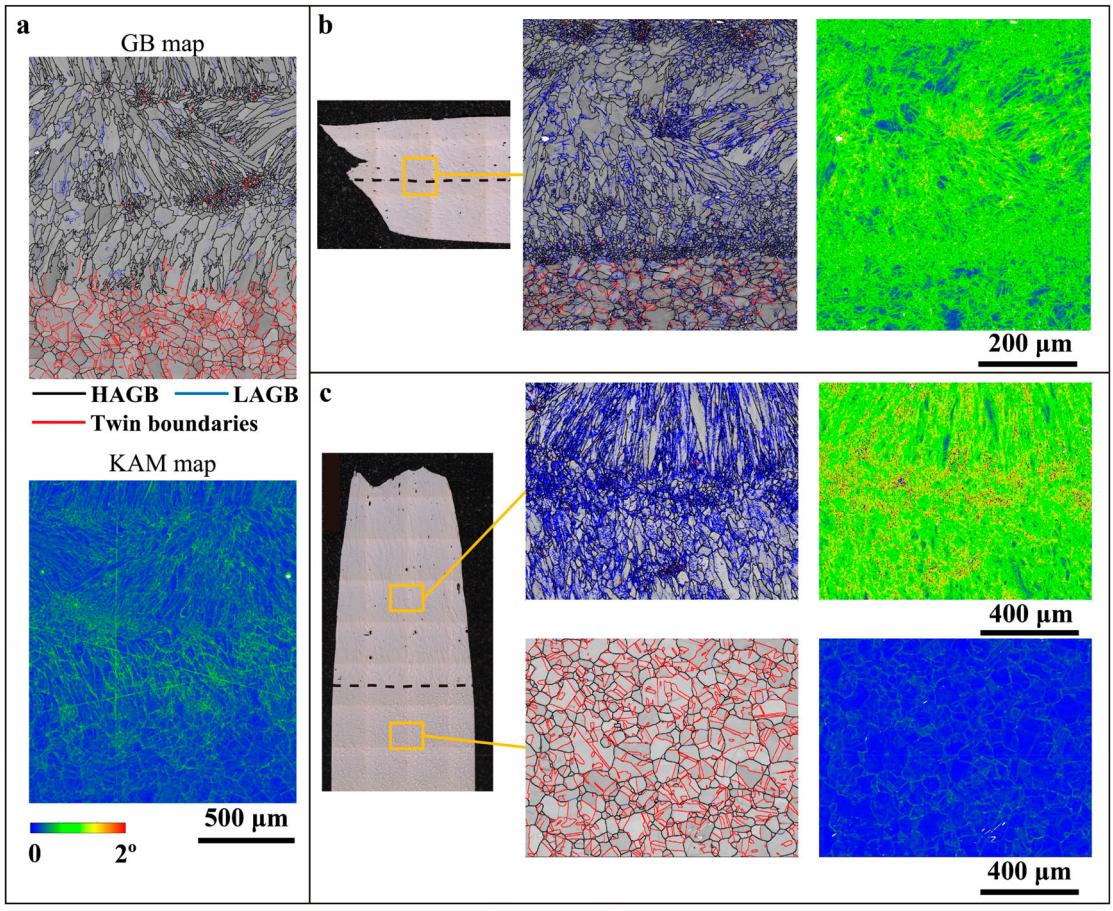

Figure 5. Comparison of the repaired microstructure before and after deformation. EBSD grain boundary map and KAM map of (a) initial microstructure, (b) horizontally deformed microstructure, and (c) vertically deformed microstructure.

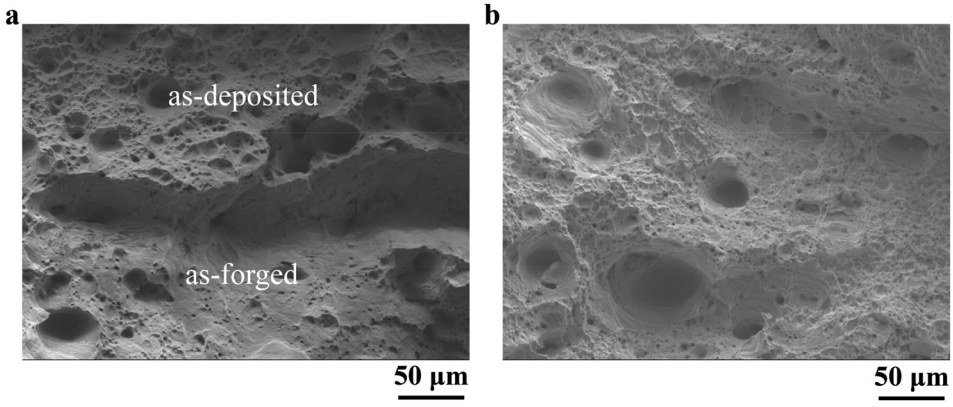

Figure 6. Fracture morphology of tensile coupons along (a) horizontal and (b) vertical loading directions, respectively.

incompatible with the components produced by additive manufacturing, otherwise it may damage the geometries which are purposely designed. Therefore, it is impractical to harden as-deposited parts by introducing deformation to increase dislocation densities as conventional manufacturing processes. Further investigation needs to be performed on improving the mechanical properties of the deposited microstructures by process modification. For instance, aging treatment can be used to harden the deposited part by precipitation, and thus increase the strength of the repaired component. Introducing nano-sized strengthening particles into the as-deposited part might be another potential option. This work provides implication for repairing marine parts, including blades, seawater vavles, and prepeller shafts, by DED in the future.

4. Conclusions

This work investigated the application of laser-DED on the repair of Monel K-500 parts with wrought microstructure. The newly deposited parts consist of large columnar grains, resulting in relatively lower tensile strength values than those of the original wrought part predominated with equiaxed grains. The Monel alloy part repaired by 1200 W laser exhibited a higher tensile strength (544.7 MPa) than that repaired by 1500 W laser (473.9 MPa). This is because employing a lower laser power is beneficial for refining the deposited microstructure and enhancing the mechanical properties. The yield strength and elongation of the Model alloy part repaired by 1200 W laser were 409.1 MPa and 35.2% along horizontal tension, both significantly surpassing the values of 353.7 MPa and 11.7% along vertical tension. Owing to the difference in the strength between the original wrought and deposited parts, upon the tensile deformation, strain exclusively accumulated in the deposited part if the loading direction was perpendicular to the bonding interface. The numerical simulation conducted in this work can be used to predict the mechanical behaviour of the repaired parts, which would be helpful in the design of the repair process. The findings shown in this work can be applied to the repair of other alloys by laser-DED with heterogeneous microstructure and anisotropic mechanical properties.

Disclosure statement

No potential conflict of interest was reported by the author(s).

Funding

This work was supported by the Economic Development Board, Singapore and DNV Singapore Pte. Ltd. through the Industrial Postgraduate Programme with Nanyang Technological University, Singapore, and the National Research Foundation, Prime Minister's Office, Singapore under its Medium-Sized Centre funding scheme through the Marine and Offshore Program.

ORCID

Kun Zhou http://orcid.org/0000-0001-7660-2911

References

[1] Ze C, Changjun H, Ming G, et al. A review on qualification and certification for metal additive manufacturing. Virtual Phys Prototyp. 2022;17(2):382–405. doi:10.1080/17452759.2021.2018938

[2] Wistance W, Jeremy L. (2018). Additive manufacturing metal 3D printing for the marine and offshore sector - paving the path from Lab into the field. In Offshore Technology Conference Asia 2018, OTCA 2018. Offshore Technology Conference. doi:10.4043/28465-ms

[3] Mohd. J, Haleem A. Additive manufacturing applications in medical cases: A literature based review. Alexandria J Med. 2018;54(4):411–422. doi:10.1016/j.ajme.2017.09.003

[4] Williams H, Butler-Jones E. Additive manufacturing standards for space resource utilization. Addit Manufact. 2019;28(June):676–681. doi:10.1016/j.addma.2019.06.007

[5] Zeng Z, Wang C, Zhen LY, et al. Influence of microstructure on stainless steel 316L lattice structures fabricated by electron beam and laser powder Bed fusion. Mater Sci Eng A. 2022;859(July):144225), doi:10.1016/j.msea.2022.144225

[6] Gebler M, Schoot Uiterkamp AJM, Visser C. A global sustainability perspective on 3D printing technologies. Energy Policy. 2014;74(C):158–167. doi:10.1016/j.enpol.2014.08.033

[7] Martin JH, Yahata BD, Hundley JM, et al. 3D printing of high-strength aluminium alloys. Nature. 2017;549(7672):365–369. doi:10.1038/nature23894

[8] Vendra L, Achanta A. (2020). Metal additive manufacturing in the oil and gas industry. Solid Freeform Fabrication 2018: Proceedings of the 29th Annual International Solid Freeform Fabrication Symposium - An Additive Manufacturing Conference: SFF 2018: 454–460.

[9] Svetlizky D, Mitun D, Baolong Z, et al. Directed energy deposition (DED) additive manufacturing: physical characteristics, defects, challenges and applications. Mater Today. 2021;49(October):271–295. doi:10.1016/j.mattod.2021.03.020

[10] Thompson SM, Linkan B, Nima S, et al. An overview of direct laser deposition for additive manufacturing; part I: transport phenomena, modeling and diagnostics. Addit Manufact. 2015;8:36–62. doi:10.1016/j.addma.2015.07.001

[11] Adrita D, Moridi A. State of the Art in directed energy deposition : from. Coatings. 2019;9(7):1–26.

[12] Zhen LY, Chengcheng W, Xiaojun S, et al. Additive manufacturing of corrosion-resistant maraging steel M789 by directed energy deposition. Mater Sci Eng A. 2022;857(August):144032), doi:10.1016/j.msea.2022.144032

[13] Svetlizky D, Baolong Z, Alexandra V, et al. Laser-based directed energy deposition (DED-LB) of advanced materials. Mater Sci Eng A. 2022;840(March):142967), doi:10.1016/j.msea.2022.142967

[14] Khorram NM, Ali TS, Fabio N. Why manufacturers adopt additive manufacturing technologies: The role of sustainability. J Cleaner Prod. 2019;222:381–392. doi:10.1016/j.jclepro.2019.03.019

[15] Pierre C, Khan T. Evolution of Ni-based superalloys for single crystal Gas turbine blade applications. Aerosp Sci Technol. 1999;3(8):513–523. doi:10.1016/S1270-9638(99)00108-X

[16] Shang Z, Xianping W, Dazhuo S, et al. Microstructure and mechanical properties of a new nickel-based single crystal superalloy. J Mater Res Technol. 2020;9(5):11641–11649. doi:10.1016/j.jmrt.2020.08.032

[17] Ramsperger M, Singer RF, Carolin K. Microstructure of the nickel-base superalloy CMSX-4 fabricated by selective electron beam melting. Metall Mater Trans A. 2016;47 (3):1469–1480. doi:10.1007/s11661-015-3300-y
[18] Everhart JL. *Engineering properties of nickel and nickel alloys*. Plenum Press; 1971. doi:10.1007/978-1-4684-1884-2
[19] Olexandra M, Kostryzhev A. Strengthening mechanisms in nickel-copper alloys: A review. Metals (Basel). 2020;10 (10):1–18. doi:10.3390/met10101358
[20] Raffeis I, Adjei-Kyeremeh F, Vroomen U, et al. Qualification of a Ni–Cu alloy for the laser powder Bed fusion process (LPBF): Its microstructure and mechanical properties. Appl Sci. 2020;10(10):3401), doi:10.3390/app10103401
[21] Marenych O, Kostryzhev AG, Pan Z, et al. Comparative effect of Mn/Ti solute atoms and TiC/Ni_3 (Al,Ti) nano-particles on work hardening behaviour in Ni–Cu alloys fabricated by wire Arc additive manufacturing. Mater Sci Eng A. 2019;753(January):262–275. doi:10.1016/j.msea.2019.03.040
[22] Chen Z, Wang C, Tang C, et al. Microstructure and mechanical properties of a monel K-500 alloy fabricated by directed energy deposition. Mater Sci Eng A. 2022;857 (November):144113), doi:10.1016/j.msea.2022.144113
[23] Terrassa KL, Smith TR, Sen J, et al. Improving build quality in directed energy deposition by cross-hatching. Mater Sci Eng A. 2019;765(July):138269), doi:10.1016/j.msea.2019.138269
[24] Li Fukun, Yuan Hao, and Liu Huijuan. 2021. "Implementation of metal ductile damage criteria in abaqus FEA." J Phys Conf Ser 1906 (1). doi:10.1088/1742-6596/1906/1/012058
[25] Farzaneh A, Khorasani M, Farabi E, et al. Sandwich structure printing of Ti-Ni-Ti by directed energy deposition. Virtual Phys Prototyp. 2022;17(4):1006–1030. doi:10.1080/17452759.2022.2096647
[26] Hansen N. Hall-Petch relation and boundary strengthening. Scr Mater. 2004;51(8 SPEC. ISS.):801–806. doi:10.1016/j.scriptamat.2004.06.002
[27] Moussa C, Bernacki M, Besnard R, et al. About quantitative EBSD analysis of deformation and recovery substructures in pure tantalum. IOP Conf Ser: Mater Sci Eng. 2015;89(1). doi:10.1088/1757-899X/89/1/012038
[28] Shamsaei N, Yadollahi A, Bian L, et al. An overview of direct laser deposition for additive manufacturing; part II: mechanical behavior, process parameter optimization and control. Addit Manufact. 2015;8:12–35. doi:10.1016/j.addma.2015.07.002